ACS APPLIED MATERIALS & INTERFACES

Research Article

www.acsami.org

Double-Stranded DNA-Graphene Hybrid: Preparation and Anti-Proliferative Activity

Dickson Joseph,[†] Shinae Seo,[‡] Darren R. Williams,[‡] and Kurt E. Geckeler*[,†,§,⊥]

[†]Laboratory of Applied Macromolecular Chemistry, Department of Nanobio Materials and Electronics (WCU), [§]School of Materials Science and Engineering, [⊥]Department of Medical System Engineering, and [‡]New Drug Targets Laboratory, School of Life Science, Gwangju Institute of Science and Technology (GIST), Gwangju 500-712, South Korea

Supporting Information

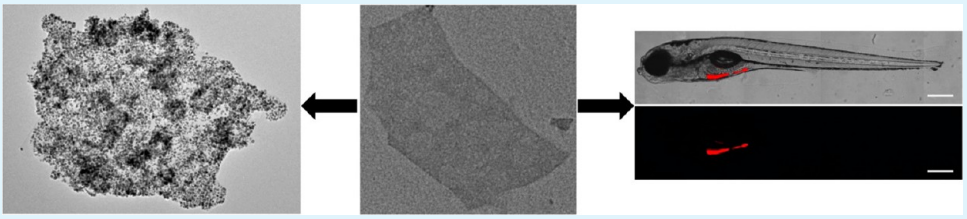

ABSTRACT: Herein, we demonstrate a simple method to prepare graphene dispersions in an aqueous solution of DNA by the sonication of bulk graphite. The use of a commercial double-stranded DNA as a stabilizer for graphite exfoliation without any chemical modification is presented. The high energy sound waves cleave a double-stranded DNA into two single-stranded DNAs. UV−vis spectral studies show that the nucleobases in the product are intact. Atomic force microscopy studies reveal that the size of the obtained nanosheets can be enriched into smaller lateral dimensions using centrifugation. Raman spectroscopy suggests that the defects found in the nanosheets induced by the sonication are edge defects, whereas the bodies of the sheets remain relatively defect free. The graphene dispersions are extremely stable over a wide range of pH values, possessing high negative zeta potential values. The anti-proliferative effect observed through in vitro cytotoxicity studies is supported by in vivo studies using the zebrafish human tumor xenograft model. The migration of cancer cells in zebrafish embryos are inhibited by the graphene nanosheet dispersion. The negatively charged nanosheet serves as a platform for the adsorption of gold nanoparticles with positively charged surfaces.

KEYWORDS: *DNA, gold nanoparticle, sonication, graphene, zeta potential, cytotoxicity, anti-proliferation*

1. INTRODUCTION

Graphene, a two-dimensional lattice of carbon with a thickness of a single atom's diameter, is currently the most extensively studied material because of its outstanding electronic, mechanical and chemical properties.[1−4] These unique properties make graphene and graphene-based materials promising candidates in applications such as electronics, photonics, energy storage, bioapplications, electrochemical devices, sensors, composite materials, paints and coating.[5−7] Graphene research has progressed rapidly because of its relatively simple and cheap pioneering laboratory procedure to obtain a high-quality product.[1] Nevertheless, the challenge for industrial applications is to produce graphene on a large scale with the same outstanding performance as the best samples obtained in research laboratories. Currently, both physical and chemical methods are employed to prepare graphene of various dimensions, shapes and quality, including mechanical exfoliation, chemical vapor deposition, epitaxial growth and liquid phase exfoliation. Graphene was discovered using mechanical exfoliation, although this method can result in pure graphene sheets, the process is not economical and is impossible for mass production.[1,5] Similarly, the yields of high-quality graphene produced by methods such as chemical vapor deposition[8] and epitaxial growth on SiC[9] are too low for large-scale application. However, liquid phase exfoliation, especially the chemical modification of graphite, has been known for years as a scalable method. The chemical modification of graphite involves the oxidation of graphite, followed by exfoliation in water to give aqueous dispersions of graphene oxide, which is later reduced chemically or by thermal treatment to graphene.[10,11] However, the oxidization process also exposes a large number of structural defects within the graphene sheets that compromise some of the properties and the unique morphology of the pristine two-dimensional hexagonal carbon lattices.[12−14] Additionally, the multistep process involves toxic oxidizing and reducing reagents, which increases the economic, safety, and environmental costs involved in large scale production.

To overcome the drawbacks of the above method, simpler liquid phase exfoliation methods have been developed to directly exfoliate graphene from graphite without oxidation or defect formation. These methods use specific solvents to exfoliate and stabilize graphene in combination with the aid of

Received: November 26, 2013
Accepted: February 20, 2014
Published: February 20, 2014

sonication, which causes the graphite to split into individual platelets, and prolonged treatment resulting in a significant fraction of monolayer sheets in the suspension, which can be further enriched by centrifugation.[15−21] However, this process also has its drawbacks because the solvents are expensive and require special care while handling. In addition, some solvents, such as N-methyl-pyrrolidone, ortho-dichlorobenzene and benzylamine have high boiling points, making it difficult to deposit individual monolayers onto the surfaces.[15,19,20] Most importantly, water, the most useful solvent of all, does not result in good dispersion of graphene as its solubility parameters lie further away from the prerequisite values.[21] This issue was addressed by exfoliating graphite in surfactant-water solutions in a manner similar to surfactant-supported carbon nanotube dispersions.[22−25] In addition to surfactants, biomolecules such as deoxyribonucleic acid (DNA), proteins, and enzymes can also be used to exfoliate graphite, as it is known to effectively debundle and disperse carbon nanotubes.[26−30]

Exfoliation of graphene in water using biocompatible materials is important because it is a necessary requirement for potential application in biological or medical fields. The best possible method to prepare such biocompatible graphene is to utilize biomolecules to directly exfoliate graphite aided by sonication. Among the biomolecules, DNA is the most popular and extensively studied material when considering the preparation of graphene-biomolecule hybrids.[7,31,32] Apart from its fundamental importance in biology, DNA is known to possess specific recognition interactions that can interact with graphene through hydrophobic adsorption and $\pi-\pi$ stacking.[33,34] There are a number of reports on the non-covalent functionalization of graphene oxide and reduced graphene oxide with DNA.[7,31,32] However, to date there are only two reports[35,36] on the direct exfoliation of graphite to graphene using DNA aided by sonication. Both groups have utilized single-stranded (ss) DNA, as a previous report suggested that double-stranded (ds) DNA resulted in less stable graphene suspensions, presumably because hydrophobic interactions with the graphene surface were sterically hindered by the base pairing of the nucleobases.[37] The researchers reported that ssDNA was obtained by heating dsDNA at 95 °C for 1−2 h to break the hydrogen bonding between the two polynucleotide strands, thereby separating them into two ssDNAs. Subsequently, the objective of our work was to prepare graphene directly from graphite with the aid of sonication in the presence of DNA. We utilized dsDNA to understand if the sonication would disrupt its double-helical conformation to form cleaved ssDNAs, which could stabilize the graphene nanosheets (GNs) by hydrophobic interactions and $\pi-\pi$ stacking. Additionally, GNs with smaller lateral dimensions were targeted as a potential successful interface with biological systems and to study its cytotoxicity behavior for biomedical applications.[31,38]

Herein we report on the exfoliation of graphite to graphene aided by sonication in an aqueous solution of dsDNA. The exfoliated GNs have average lengths of 130 nm and thicknesses of 0.8 nm, confirmed using AFM and Raman studies. Additionally, the dispersion exhibits high pH stability in a wide range of pH values (3 to 13). MTT assays were used to study the in vitro cell viabilities of fibroblasts and cancer cells after treatment with the DNA-supported GNs to check their cytotoxicity and their antimigration properties for future biomedical applications. In vivo studies were carried out using a zebrafish human tumor xenograft model to understand the anti-proliferation properties of the GNs by studying the cancer cell migration in zebrafish embryos. The electrostatic interaction between the GNs and gold nanoparticles was studied by adsorbing gold nanoparticles with a positive surface charge, which were prepared using a basic protein, to the surface of the GNs.

2. EXPERIMENTAL SECTION

2.1. Materials and Methods. Graphite powder (<20 μm), double-stranded DNA (from Herring testes, sodium salt), calf histone (HIS), ethyl 3-aminobenzoate methanesulfonate salt (tricaine), and taxol used for the experiments were obtained from Sigma Aldrich, USA. 1,1′-dioctadecyl-3,3,3′,3′-tetramethyl-indocarbocyanine perchlorate (DiI) was purchased from Invitrogen. Deionized (Milli-Q grade) water was used to prepare all of the solutions. Sonication was performed with an ultrasonic processor (Sonics and Materials, Inc., model VC 750) equipped with a standard tip probe (diameter: 13 mm). The microwave system utilized a 10 mL pressurized vial and cap that automatically vented when the vial internal pressure reached 300 psi. Absorption spectra were recorded on a PerkinElmer UV−vis spectrophotometer (Lambda 750). Atomic force microscopy (AFM) (Park System Corp, XE-Bio) in the contact mode was used to analyze the thickness and length of the GNs. All AFM images were processed using XEI software provided by Park System Corp. The samples for AFM measurements were prepared by spotting 50 μL of a sample onto a freshly cleaved mica surface. The mica substrate was carefully tilted to allow the droplet to spread evenly on the mica surface. After 10 minutes, the sample droplet was removed by rinsing with deionized water, and the mica surface was dried with compressed air before imaging. Raman scattering studies were carried out using a Renishaw InVia Raman spectrometer, with an excitation wavelength of 514 nm. The zeta potential of the dispersions in aqueous solution was recorded by light scattering using an ELS 8000 (Photal, Otsuka Electronics Co. Ltd, Japan).

2.2. Preparation of DNA-Supported GNs and Gold Nanoparticle Hybrids. In a typical experiment, a 10 mL DNA solution (0.5 mg/mL) was mixed with 20 mg of graphite powder to yield a 1:4 DNA:graphite mixture. The mixture was sonicated (cycles of 5 s ON and 1 s OFF, the power of the ultrasonic tip was 60 %, 750 W) for 6 h in an ice bath using a standard probe, resulting in a fine black dispersion. The final products of the dispersion were collected from the supernatant by employing a double-step centrifugation, 2500 rpm for 30 min, followed by 5000 rpm for 30 min. The first centrifugation removed the un-exfoliated graphite and multilayered graphene, which led to a stable dispersion. The second centrifugation separated GNs of smaller dimensions. Therefore, we considered these steps to be the exfoliation and dispersion limits, and we used data from these steps to calculate the graphene concentration in the dispersions. The histone-coated AuNPs were prepared in 10 mL capped vials containing 5 mL of an aqueous protein solution (1 mg/mL), $KAuCl_4$ (0.025 mL, 0.1 M) and $AgNO_3$ (0.005 mL, 0.1 M). The vials were microwaved at 250 W and 120 °C for 10 min. After cooling to 25 °C, the resultant colloidal AuNPs were centrifuged at 15000 rpm for 15 min, the residue was collected and mixed with 1 mL of the above obtained graphene dispersion. The mixture was then sonicated under mild conditions for 15 min and then allowed to stand undisturbed for 12 h. The product was collected as a residue obtained from centrifugation at 15000 rpm for 60 min and then characterized.

2.3. Cell Culture and Cell Viability Test (MTT Assay). Mouse embryonic fibroblasts (NIH-3T3) and human colorectal cancer cells (HCT-116) were routinely maintained in Dulbecco's Modified Eagles Medium (DMEM) supplemented with 10 % fetal bovine serum (FBS, SIGMA) and 1 % antibiotic-antimycotic (GIBCO). The NIH-3T3 cells were originally obtained from the Korean Cell line Bank (Seoul, Korea) and HCT-116 cells were purchased from the American Type Culture Collection. All of the cells were cultured in a humidified atmosphere containing 5% CO_2 and maintained at 37 °C. To assess the effect of GNs on the viability percentages of the cells, MTT [3-(4,

5-dimethylthiazol-2-yl)-2, 5-diphenyltetrazolium bromide] colorimetric assays were performed. The cells were seeded in 96-well plates at a density of 5 x 10^4 cells/well and incubated for 24 h in 200 μL of culture media at 37 °C. On the following day, the cells were further treated with different concentrations of graphene samples prepared in fresh media, substituting the prior culture media in which the cells were seeded. After a 24 h incubation period, the media were removed, the cells were rinsed with PBS, and again incubated with 40 μL of MTT solution for 4 h. The supernatant was then removed carefully, and dimethyl sulfoxide (Junsei Chemical Co. Ltd) was added to each well to dissolve the purple formazan produced by the MTT. The absorbance was measured using a microplate reader (FL600, Microplate Fluorescence Reader, Bio-Tek Company) at a wavelength of 570 nm. All experiments were carried out in triplicates. The concentration of the sample causing 50% inhibition of proliferation of the cells (IC50) was determined by plotting the percentage of cell viability versus the sample concentrations.

2.4. Zebrafish Human Cancer Cell Xenograft Model. Zebrafish were maintained in accordance with standard guidelines. Care and treatment of the zebrafish were conducted in accordance with guidelines established by the Animal Care and Ethics Committee of the Gwangju Institute of Science and Technology, Republic of Korea. Zebrafish embryos were obtained using standard mating conditions and staged for cell xenoplantation at 48 h post fertilization. Each treatment group was comprised of 20 embryos. After staining of the cancer cells, the embryos were de-chorionized using micro-forceps and anesthetized with 0.0016 % tricaine and positioned on their right side on a wet 1.0 % agarose pad. Tumor cells were detached from the culture dishes using 0.05 % trypsin-EDTA and washed twice with PBS at room temperature. The cells were stained with 2 μg/mL DiI diluted in PBS and washed four times: once with FBS, twice with PBS and then once with 10 % FBS diluted in PBS. The cells were kept on ice before injection. Cancer cells were counted by microscopy, suspended in 10% FBS and injected into the center of the yolk sac using an injector (PV820 pneumatic picopump, World Precision Instruments) equipped with borosilicate glass capillaries (World Precision Instruments, FL, USA). Injected embryos were transferred to a 96-well plate (one embryo/well) containing the GNs in 200 μL E3 media (without methylene blue). The number of embryos exhibiting cancer cell dissemination from the injection site was counted using upright fluorescence microscopy (Leica DM2500 Microscope, Germany). Representative pictures were also captured using upright microscopy. The student's t-test was used for comparison between experimental groups (Microsoft Excel). P values of 0.05 were considered significant.

3. RESULTS AND DISCUSSION

The ultrasonication process implodes the cavitation bubbles formed in the solution, creating high pressures and temperatures, while the implosions also cause violent high-speed collisions between particles.[39] We speculate that this extreme transient condition, produced during acoustic cavitation, dissociates the hydrogen bonding between the dsDNA nucleobases leading to two ssDNA. To investigate the concentration of DNA in the dispersion after sonication, a DNA solution was sonicated for 6 h without graphite, and the solution was then studied using UV−vis spectroscopy. DNA exhibits a strong absorbance at 260 nm,[29] and this absorbance peak was also present in the DNA solution sonicated for 6 h. The nucleobases containing the conjugated π bonds are responsible for the strong absorbance peak at 260 nm, the presence of this peak indicates that the structural integrity of the nucleobases are retained even after sonication for 6 h. To determine the actual DNA concentration after sonication, samples with five different and known DNA concentrations from 0.1 to 0.5 mg/mL were prepared and studied using a UV−vis spectrophotometer. The absorbance values of the samples were recorded and, as expected, the absorbance

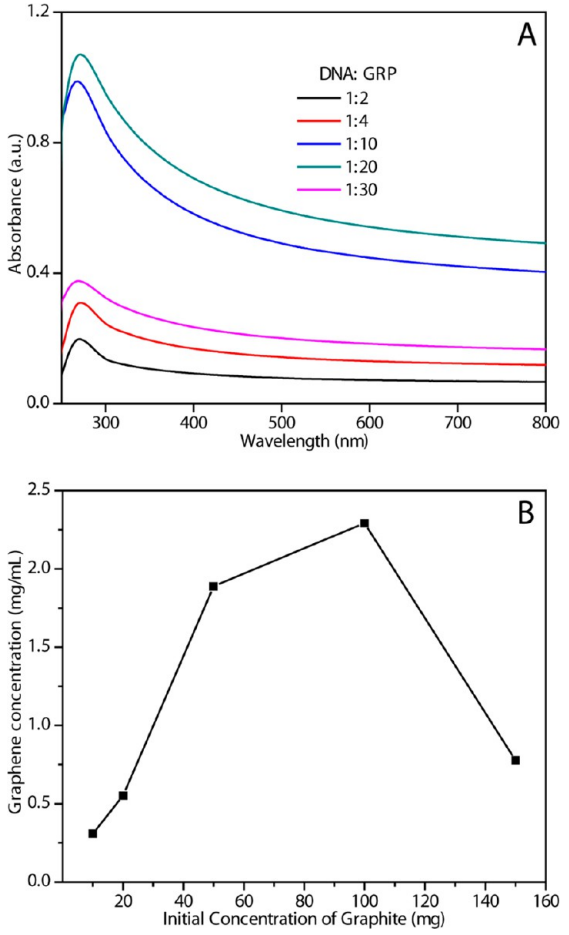

Figure 1. (A) Absorption spectra of the graphene dispersions and (B) graphene concentration plot as a function of initial graphite concentration.

intensity was dependent on the DNA concentration. Figure S1 in the Supporting Information shows a comparative absorption plot of the known DNA concentrations and the unknown sonicated DNA sample. The concentration of the DNA in the sonicated solution was approximately 0.5 mg/mL, which was the initial concentration used for the study. Therefore, the above study clearly demonstrates that even though the sonication causes the cleavage of the hydrogen bonds between the nucleobases, it does not affect the structure and concentration of the nucleobases in the dispersion.

The graphene concentrations in the dispersions were determined by UV−vis absorption spectroscopy as follows.[22] The supernatant obtained after the second centrifugation step was freeze dried, and the powder collected and weighed. Five samples of different and known concentrations (mg/mL) were prepared and their UV−vis absorption at 660 nm was measured (see Figure S2A in the Supporting Information). The concentrations and the 660 nm absorbance afforded the linear calibration curve shown in Figure S2B in the Supporting Information. The extinction coefficient, α_G = 13.67 mL mg^{-1} cm^{-1}, obtained from the slope of the calibration curve, was used to determine the sample concentrations through the Beer−Lambert law ($A = \alpha_G C_G l$). To determine the maximum concentration of graphene that can be obtained by this method, we carried out reactions with variable initial graphite concentrations, followed by absorption studies. Sonication was performed for 6 h with a fixed concentration of DNA, 0.5

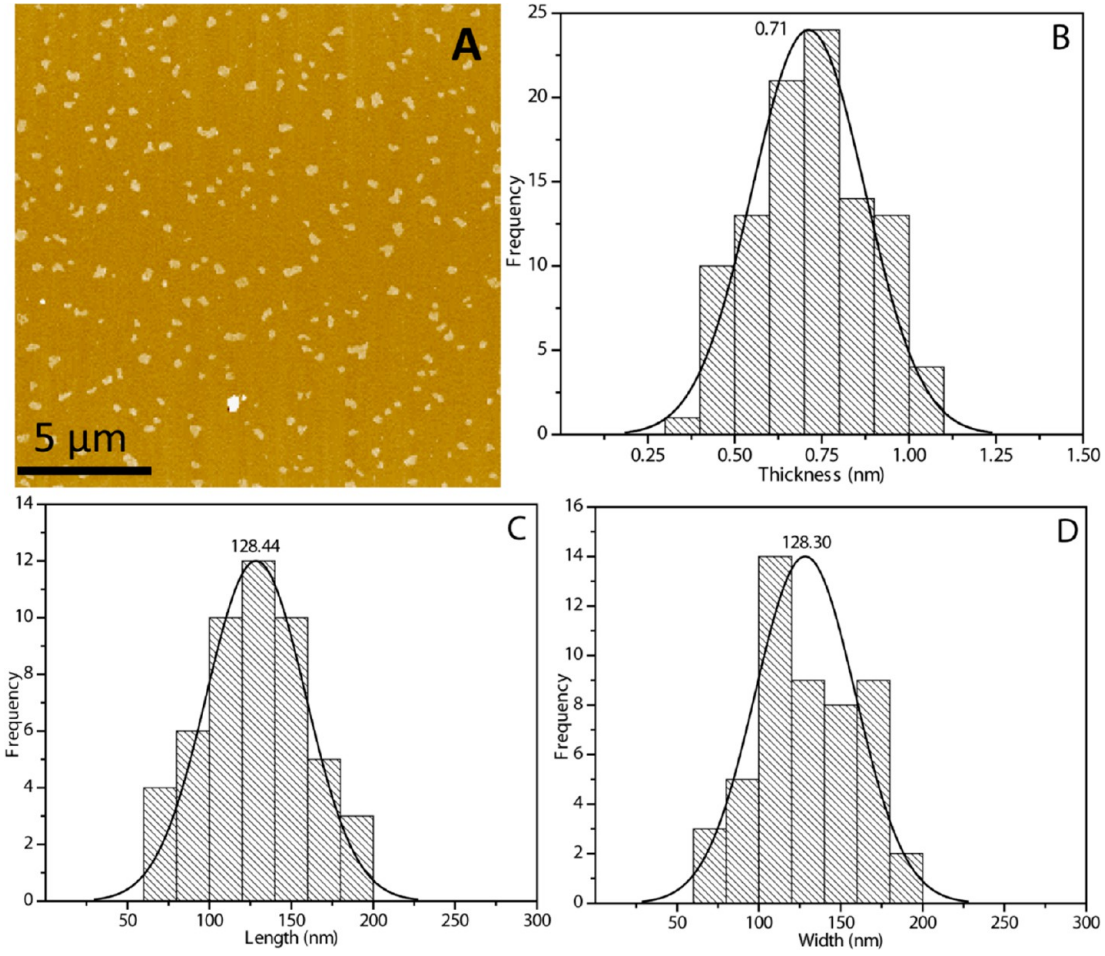

Figure 2. Morphological analysis of nanosheets in DNA-G2: (A) AFM image of graphene nanosheets. Statistical analysis of the nanosheets: (B) thickness, (C) length, and (D) width.

mg/mL, in a 10 mL aqueous solution, whereas the initial graphite feed amounts varied from 10 to 150 mg/mL. The black dispersion obtained after the sonication was centrifuged and the resultant dispersion was subjected to absorption studies (Figure 1A). The absorbance value at 660 nm for each of the products was used to determine the respective concentration of graphene in the dispersion. The maximum graphene concentration (2.29 mg/mL, Figure 1B) was achieved with an initial graphite feed of 100 mg, while initial graphite feeds above 100 mg resulted in poor graphene dispersion. We speculate that this poor dispersion arose from insufficient penetration of the sound waves into the highly concentrated graphite solution. Therefore, cavitation, which is responsible for the exfoliation process, could not occur.

The morphology, thickness, length, width and aspect ratio of the GNs were explored using AFM. A large-area image of the GNs is shown in Figure 2A. The AFM images clearly indicated that the GNs were small, possessing dimensions less than 200 nm. Dimensions (length, width, aspect ratio, and thickness) for 50 graphene flakes were measured, and the statistical analyses are plotted in Figures 2B–D. The average length and width of the GNs were both 128 nm, corresponding to an aspect ratio of 1. The average thickness of the GNs was 0.71 nm, corresponding to approximately single or bilayer GNs.[40] To compare the dimensions of the 2nd centrifugate shown above with the first centrifugate, AFM studies were also carried out on the 1st centrifugate sample. Results suggest that the GNs were slightly thicker and larger in lateral dimension, with an average thickness of 1.3 nm and length of 235 nm (Figure 3).

To obtain graphene sheets with smaller lateral dimensions, we carried out sonication for 6 h using a high power sonic tip. During the sonication process, as the large graphite crystallites are exfoliated and cut into smaller sheets, the introduction of edge defects was unavoidable. The quality of the GNs was assessed using Raman spectroscopy, which allowed a non-destructive identification of the number of layers in the GNs. Comparative Raman studies for the 1st and the 2nd centrifugate were conducted to develop a better understanding of the defects induced by the sonication. Raman spectra for the graphite powder and the DNA graphene samples, DNA-G1 (1st centrifugate) and DNA-G2 (2nd centrifugate), are shown in Figure 4. The three most intense peaks were observed at ~1350 cm^{-1} (D band), ~1580 cm^{-1} (G band) and ~2700 cm^{-1} (2D band).[15,19,23] In addition to the G and 2D peaks in DNA-G, the presence of the significant D peak, the D' shoulder peak and the combination mode D + D′ at 2950 cm^{-1} confirmed graphite exfoliation.[41] The presence of the D band suggested either edge or topological defects in the sheets[15,19,23] because this sp^2-carbon breathing mode requires a defect for its activation. The D-band intensity is directly related to the amount of disorder in the graphene sheets. The size of the defect-free sp^2 cluster regions is inversely related to the D band to G band intensity ratio (I_D/I_G).[42] The I_D/I_G for DNA-G1 and DNA-G2 samples was calculated to be 0.61 and 0.79,

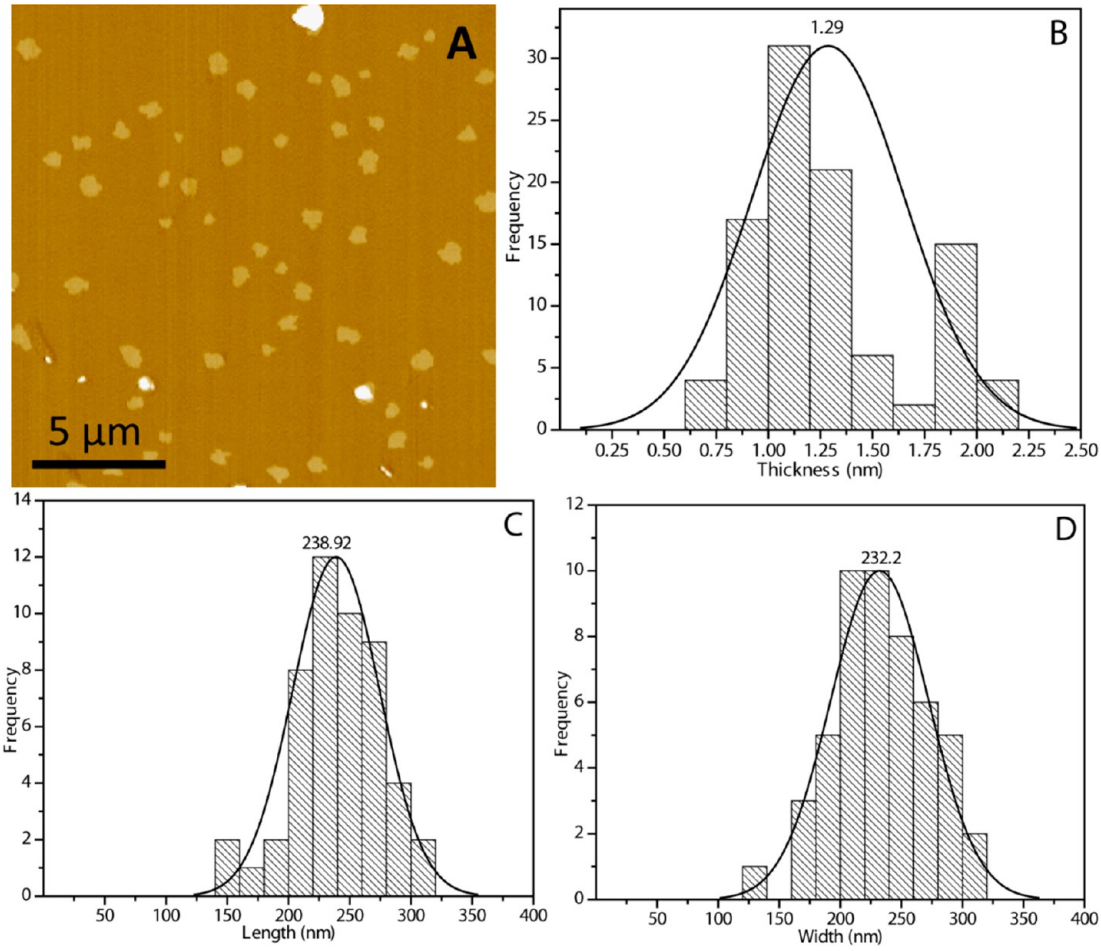

Figure 3. Morphological analysis of nanosheets in DNA-G1: (A) AFM image of graphene nanosheets. Statistical analysis of the nanosheets: (B) thickness, (C) length, and (D) width.

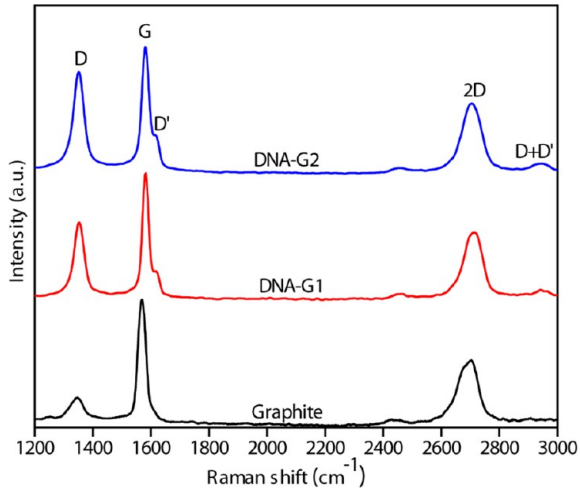

Figure 4. Raman spectra of graphite powder and the DNA-supported graphene nanosheets.

respectively, indicating that relatively defect-free GNs were produced. These values are significantly lower than the graphene sheets obtained from GO reduction by hydrazine ($I_D/I_G \approx 1.44$).[11] Therefore, our approach for exfoliating graphite in water using DNA produced GNs with significantly fewer defects. However, it remains to be determined if these defects are on the basal plane of the graphene sheets or defects associated with new edges. Coleman and coworkers reported that as the centrifugal rotation times are increased for samples prepared using the same sonication time, the size of the sheets decrease and the I_D/I_G values increase. They concluded from this study that the observed defects are associated with the edges and the bodies of the sheets are relatively defect free.[19] A similar behavior is also observed in our work, therefore, we compared the I_D/I_G values for DNA-G1 and DNA-G2 and found that more defects are induced in the later sample. This is because DNA-G2 is centrifuged at a higher speed in comparison to DNA-G1, resulting in sheets with smaller size to be retained in the dispersion (Figure 4). Hence, these smaller sheets have more edges per unit mass resulting in an increase in edge defect population, which concurs with the above report. Additionally, the lack of G-band broadening also implied that the D-band defects originate from new edges and not from basal-plane defects. The 2D peak appeared because of the activation of two phonons with identical momentum. No defects are required for this activation; the 2D band is always observed, even when no D band is present. Green and Hersam reported that as the graphene sheet thickness increased, I_{2D}/I_G decreased steadily from a high of 2.1 ± 0.2 for single-layer graphene to 0.8 ± 0.1 for quadruple-layer graphene.[23] We collected spectra from at least 15 different locations and determined the I_{2D}/I_G mean value as 0.6, which corresponded to approximately 5 or less layers. Because we used a 2 μm laser beam and the prepared GNs had dimensions less than 150 nm,

we believe that a large number of sheets were exposed. Moreover, the GNs may stack during the Raman sample preparation and result in single or bilayer graphene appearing as three or more layers. Therefore, the Raman spectrum obtained was a cumulative spectrum of 2 μm radius sheets. By comparing the AFM and the Raman data, we confirmed that the number of layers in the GNs was less than 3.

Understanding the correlation between pH and the zeta potential is important to understanding how the dispersion would behave in the human body, which differs with varying pH conditions. Zeta potential is the electrical potential difference between the dispersion medium and the stationary layer of fluid attached to the dispersed particle. In other words, it is the overall charge a particle acquires in a specific medium. The magnitude of the zeta potential gives an indication of the potential stability of the colloidal system. If all the particles have a large negative or positive zeta potential, they will repel each other, resulting in dispersion stability. If the particles have low zeta potential values, then there is no force to prevent the particles from coming together and the dispersion is unstable. A dividing line between stable and unstable aqueous dispersions is generally observed at either +30 or −30 mV. Particles with zeta potentials more positive than +30 mV or more negative than −30 mV are normally considered stable. The most important factor affecting the zeta potential is pH. We observed in a previous study, related to lysozyme-supported graphene, that as we added an acidic solution to the dispersion, the nanosheets acquired more positive charge. When a basic solution was added, there was a negative charge buildup on the nanosheets. The zeta potential versus the pH curve was positive at low pH values and negative at high pH values. There was a point at which the curve passed through zero zeta potential that lead to a highly unstable dispersion, and a clear solution was observed (unpublished results). This behavior was also observed in a similar study done by our group with carbon nanotubes dispersed using lysozyme.[30] The pH sensitivity of the DNA-supported graphene dispersions was analyzed by subjecting the aqueous dispersion to pH-dependent zeta potential titration studies using a zeta potential analyzer. The negative zeta potential values in Figure 5 indicate that the GNs are negatively charged. A low negative zeta potential value at pH of 1 is observed and, as the pH increased, the values also increased, coming to almost a constant value between pH values of 7 and 13. Under highly acidic conditions, the concentration of H^+ ions in the dispersion increases, these are attracted by the negatively charged GNs, which lead to a low negative zeta potential value. When the concentration of H^+ ions in the solution is decreased with an increase in pH (3 to 7), the relative number of positive charges in the dispersion decreases, thereby leading to higher negative zeta potential values. Above a pH of 7, when OH^- ions are replaced by H^+ ions in the dispersion, there is no substantial change in the zeta potential values, which shows that OH− ions are repelled by the nanosheets and are unaffected. It is interesting to note that the zeta potential values lie above −30 mV at all of the pH values expect a pH value of 1, which corresponds to high stability. These results clearly demonstrate that the GNs contain a negative surface charge that is stable over a long range of pH values. Because the DNA is highly polymerized and contains a large number of negative phosphate groups, it is not possible for the GNs to attain a dominant positive surface charge, even at the highest H^+ ion concentrations.

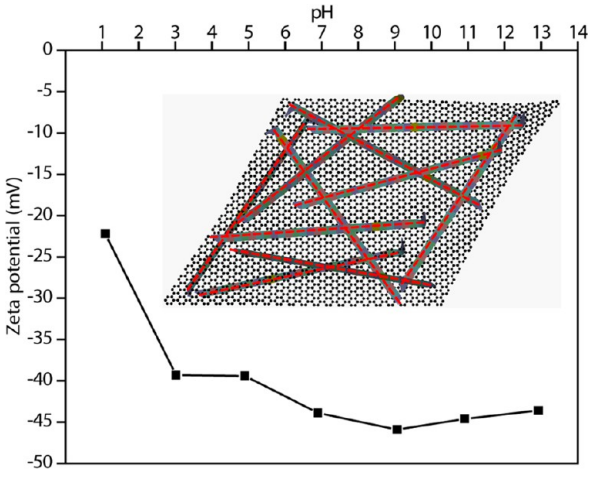

Figure 5. Variation in the zeta potential of DNA-supported graphene nanosheets as a function of the pH in the aqueous medium. The inset shows the pictorial representation of the negatively charged DNA-supported graphene nanosheets.

The presence of a dominant negative charge on the GNs is an interesting feature to study for bioapplications, as reports suggest that the negatively charged nanomaterials are internalized by the cells to a lesser extent than their positively charged counterparts.[43−45] Xia and coworkers reported that when positively charged gold (Au) nanospheres are attached to a negatively charged cell surface, the cell membrane will attempt to maintain the original charge distribution by getting rid of the attached Au nanospheres through endocytosis or other pathways that cause the cell membrane to lose its rigidity. Thus, positively charged Au nanospheres will be internalized more easily by the cells than other types of Au nanospheres.[43] Compared to the negatively charged cell surface, positively charged surface sites are scarcer on the plasma membrane, but previous reports have revealed a mechanism by which anionic nanoparticles could be absorbed.[44] The negatively charged nanoparticles that approach the cell surface are repelled by the negatively charged cell surface, which leads to a cluster formation that binds nonspecifically onto the cationic sites of the plasma membrane, resulting in subsequent endocytosis. Hence, negatively charged nanoparticles are internalized by cells but to a lesser extent than that of the positively charged nanoparticles.[45] This was confirmed in our previous study on protein-supported graphene, where the positively charged nanoparticles exhibited lower cell viability. Therefore, we expected the DNA-supported GNs to show better biocompatibility and higher cell viability; hence, cytotoxicity studies were carried out to evaluate their biocompatibility and cytotoxicity for its potential use in biomedical applications. The in vitro cytotoxicity of the samples DNA-G1 and DNA-G2 were investigated by conducting MTT assays with mouse embryonic fibroblasts (NIH-3T3) and human colorectal cancer cells (HCT-116) at four different concentrations. DNA-G1 showed higher cell viability towards both the cell lines, whereas DNA-G2 displayed lower cell viability with IC50 values of 72 and 47 μg/mL for NIH-3T3 and HCT-116, respectively. We speculate that this difference in cell viability is a result of the difference in the lateral dimensions and thickness of the GNs. The average lateral dimensions of the GNs in DNA-G2 are 100 nm smaller and 0.6 nm thinner than DNA-G1, thus they are internalized by the cells with greater ease. DNA-G1 exhibited a higher IC50 value for fibroblasts (72 μg/mL) than for the cancer cell line

(47 μg/mL), which clearly indicates that the GNs were more toxic to the cancer cells than the fibroblasts (Figure 6). The

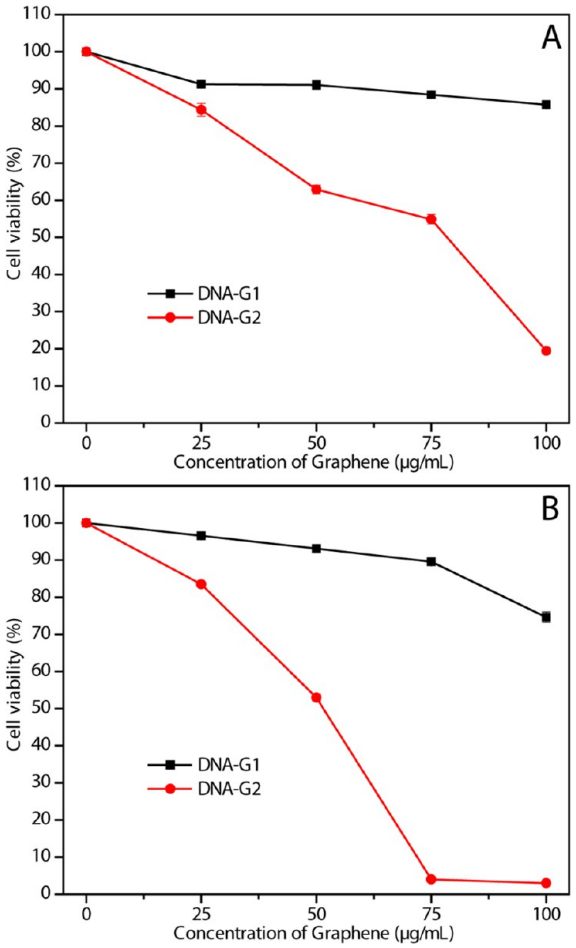

Figure 6. Cell viability studies using MTT assay on (A) NIH-3T3 and (B) HCT116 cells treated with nanosheets prepared using DNA in aqueous solution.

differences in cell viability can be explained by the zeta potential values of the dispersions at a pH of 5 (acidic pH, pH in cancer cells) and a pH of 7 (neutral pH, pH in normal cells).[46] The zeta potential values at pH values of 5 and 7 were −39.4 and −43.9, respectively. Although this difference might look small, it is clear that the GNs containing fewer negative charges are internalized easier than the GNs with a higher negative charge. Thus, because of the lower negative charge on GNs at a pH of 5, the cancer cells internalize a greater number of GNs, which disrupts the signaling process and leads to cell death. Comparatively, the normal cells with a pH of 7 internalize a fewer number of GNs, resulting in fewer cell deaths.

Preventing metastasis, the spread of cancer cells from a primary tumor to a secondary site, represents an important therapeutic approach to cancer treatment.[47] To assess the antiproliferative effect of the GNs in vivo, we studied the cell migration, the first step in metastasis, using the zebrafish human tumor xenograft model. In zebrafish cancer models, tumors can develop at various organ sites and show striking histologic and genetic similarities with their human cancer counterparts. Moreover, this model has established itself as a validated and convenient assay for testing anticancer drug candidates *in vivo*. In addition, zebrafish is a relevant vertebrate platform for predicting toxicological effects in mammals.[48−50] The optimal concentrations of the samples used for these studies was obtained from the in vitro cytotoxicity studies for the HCT-116 cancer cells. The concentrations, 50 and 75 μg/mL, were chosen based on the IC50 and IC30 values, respectively. Before carrying out the antimigration activity studies, the biocompatibility of the GNs were studied by placing zebrafish embryos at 50 and 75 μg/mL for three days at a temperature of 31 °C. After 3 days, it was observed that all the embryos were alive and healthy, confirming that the GNs are highly biocompatible. For antimigration studies, the cancer cells were injected into the yolk-sac of the embryos and incubated at 31 °C for three days after which the studies on the migration of the cancer cells were complete. For a comparative study and as a standard, similar experiments were carried out with 50 nM Taxol, a commercially available anticancer drug. Xenografted embryos exhibited 68 ± 5.0 % (P value = 0.010) and 74 ± 13.2 % (P value = 0.014) (see Figure S3 in the Supporting Information) of cancer cell dissemination by 50 μg/mL and 75 μg/mL, respectively, for GNs treatment. The control group (untreated) and the Taxol treated embryos showed 82 ± 6.7 % and 67 ± 4.7 % of embryos with cancer cell dissemination, respectively. Representative pictures taken at 6 days post injection are shown in Figure 7. These results suggest that the 50 μg/mL graphene sample inhibits the cancer cell proliferation in vivo, resulting in decreased cancer cell dissemination similar to that of 50 nM

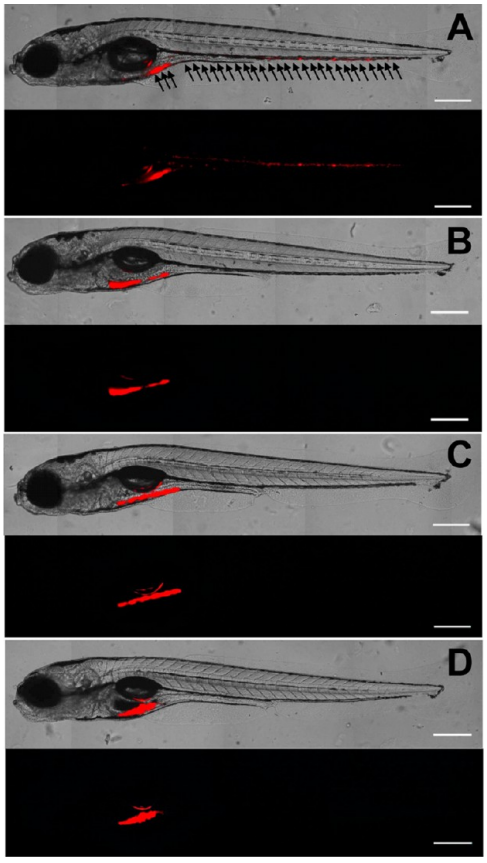

Figure 7. Representative fluorescent images and merged DIC:fluorescent images showing effect of (A) control, (B) 50 nM Taxol, (C) 50 and (D) 75 μg/mL of graphene nanosheets on xenografted cancer cell dissemination. Arrows indicates tumor foci disseminated from the injection site (yolk sac). Bar = 200 mm.

dx.doi.org/10.1021/am405378x | ACS Appl. Mater. Interfaces 2014, 6, 3347−3356

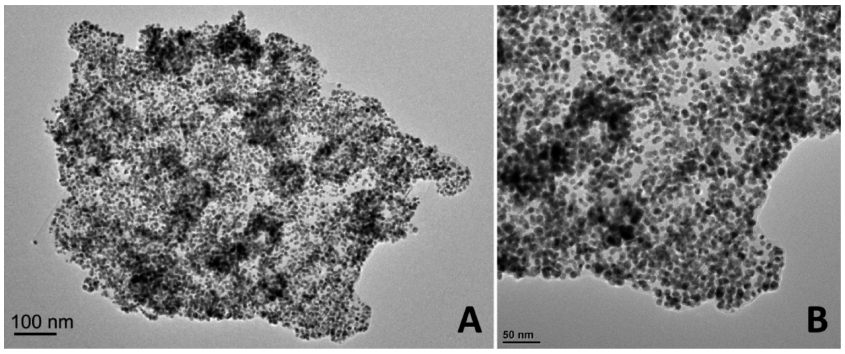

Figure 8. TEM images of the graphene nanosheet/gold nanoparticles hybrid at different magnifications.

Taxol. Although the 50 μg/mL inhibits the cancer cell proliferation by 14 % compared to the control, the 75 μg/mL showed only 8 % inhibition. This could be a result of the agglomeration of the GNs inside the embryo as observed in Figure 7D, preventing them from internalizing into the cancer cells. Therefore, the in vitro and in vivo studies suggest that if appropriate concentrations are formulated, these DNA-supported GNs on their own can be used in cancer therapy.

Graphene-based hybrids, especially metal-nanoparticle hybrids, have gained significant interest in energy and sensing applications.[51] To study whether the prepared negatively charged GNs could be used to electrostatically adsorb positively charged nanomaterials, we prepared gold nanoparticles (AuNPs) using histone, a protein that associates with DNA in the nucleus and helps condense it into chromatin. Histones are basic proteins, and their positive charges allow them to associate with the negatively charged DNA. The GNs and AuNPs with zeta potentials of −61.29 and +49.09 mV, respectively were prepared separately and mixed followed by mild sonication. The mixture was then allowed to stand overnight and was analyzed using TEM. Figure 8 shows the TEM image of a single graphene sheet that has a uniform and large number of gold nanoparticles with a diameter of 12 nm adsorbed onto the graphene. It was surprising to observe that the size of the graphene sheet was increased, we speculate that this could be a result of the layer-by-layer self-assembly of the nanoparticle embedded in the GNs.[52] The zeta potential of the product was −45.10, which shows that the high negative zeta potential of the graphene nanosheets was lowered on adsorption of the positively charged gold nanoparticles. Although these results show that positively charged gold nanoparticles can be adsorbed onto GNs, more information, such as adsorption studies on negatively charged AuNPs and other metal or metal oxide nanoparticles is still needed to understand the adsorption properties of these negatively charged GNs.

4. CONCLUSION

In summary, we have developed a simple method to directly exfoliate graphene from graphite in the aqueous phase with the assistance of dsDNA. The high energy produced during acoustic cavitation dissociates the hydrogen bonding between the dsDNA nucleobases resulting in two separate ssDNAs. These ss-deoxyribonucleotides then interact with the exfoliated graphene through hydrophobic forces and non-covalent π−π bonding, preventing the graphene from restacking or agglomerating. The hydrophilic sugar-phosphate backbone aids the dispersion of graphene in water and results in stability for more than a year. The negative charge on the surface of the GNs was confirmed by pH-dependent zeta potential analysis. UV−vis spectroscopic analysis was used to determine the concentration of graphene in the dispersion and a maximum concentration of 2.29 mg/mL was obtained using this method. As the lateral dimensions of the sheets become smaller, an increase in the defects was observed, Raman analysis confirmed that these defects were primarily edge defects, not basal-plane defects. In vitro cytotoxicity studies revealed lower cell viability towards cancer cells in comparison to fibroblasts. In vivo results show that the GNs are highly biocompatible and display dose-dependent inhibition of cancer cell dissemination in the zebrafish xenograft model. Therefore, by formulating appropriate concentrations, these GNs can be used as anti-proliferative agents. The negatively charged nanosheet adsorbs positively charged gold nanoparticles, which shows promise for toxic metal ion adsorption and the nanoparticle hybrids for energy and sensing applications. The prepared GNs also show promise for use in biomedical applications because of their high stability and biocompatible DNA surface.

■ ASSOCIATED CONTENT

Ⓢ Supporting Information

Determination of DNA concentration, time and concentration dependent absorption spectra of the graphene dispersions, plot representing cancer cell dissemination. This material is available free of charge via the Internet at http://pubs.acs.org.

■ AUTHOR INFORMATION

Corresponding Author

*E-mail: keg@gist.ac.kr. Phone: + 82-62-715-2316. Fax: +82-62-715-2338.

Notes

The authors declare no competing financial interest.

■ ACKNOWLEDGMENTS

This work was supported by the WCU program through a grant provided by the Ministry of Education, Science and Technology (MEST) of Korea (Project R31-10026).

■ REFERENCES

(1) Novoselov, K. S.; Geim, A. K.; Morozov, S. V.; Jiang, D.; Zhang, Y.; Dubonos, S. V.; Grigorieva, I. V.; Firsov, A. A. Electric Field Effect in Atomically Thin Carbon Films. *Science* **2004**, *306*, 666−669.

(2) Geim, A. K. Graphene: Status and Prospects. *Science* **2009**, *324*, 1530−1534.

(3) Bolotin, K. I.; Sikes, K. J.; Jiang, Z.; Klima, M.; Fudenberg, G.; Hone, J.; Kim, P.; Stormer, H. L. Ultrahigh electron mobility in suspended graphene. *Solid State Commun.* **2008**, *146*, 351−355.
(4) Lee, C.; Wei, X.; Kysar, J. W.; Hone, J. Measurement of the Elastic Properties and Intrinsic Strength of Monolayer Graphene. *Science* **2008**, *321*, 385−388.
(5) Novoselov, K. S.; Falko, V. I.; Colombo, L.; Gellert, P. R.; Schwab, M. G.; Kim, K. A roadmap for graphene. *Nature* **2012**, *490*, 192−200.
(6) Hong, J.-Y.; Jang, J. Micropatterning of Graphene Sheets: Recent Advances in Techniques and Applications. *J. Mater. Chem.* **2012**, *22*, 8179−8191.
(7) Zhang, H.; Gruner, G.; Zhao, Y. Recent Advancements of Graphene in Biomedicine. *J. Mater. Chem. B* **2013**, *1*, 2542−2567.
(8) Reina, A.; Jia, X.; Ho, J.; Nezich, D.; Son, H.; Bulovic, V.; Dresselhaus, M. S.; Kong, J. Large Area, Few-Layer Graphene Films on Arbitrary Substrates by Chemical Vapor Deposition. *Nano Lett.* **2008**, *9*, 30−35.
(9) Berger, C.; Song, Z.; Li, T.; Li, X.; Ogbazghi, A. Y.; Feng, R.; Dai, Z.; Marchenkov, A. N.; Conrad, E. H.; First, P. N.; de Heer, W. A. Ultrathin Epitaxial Graphite: 2D Electron Gas Properties and a Route toward Graphene-Based Nanoelectronics. *J. Phys. Chem. B* **2004**, *108*, 19912−19916.
(10) Park, S.; Ruoff, R. S. Chemical Methods for the Production of Graphenes. *Nat. Nanotechnol.* **2009**, *4*, 217−224.
(11) Tung, V. C.; Allen, M. J.; Yang, Y.; Kaner, R. B. High-Throughput Solution Processing of Large-Scale Graphene. *Nat. Nanotechnol.* **2009**, *4*, 25−29.
(12) Eda, G.; Fanchini, G.; Chhowalla, M. Large-Area Ultrathin Films of Reduced Graphene Oxide As a Transparent and Flexible Electronic Material. *Nat. Nanotechnol.* **2008**, *3*, 270−274.
(13) Shin, H.-J.; Kim, K. K.; Benayad, A.; Yoon, S.-M.; Park, H. K.; Jung, I.-S.; Jin, M. H.; Jeong, H.-K.; Kim, J. M.; Choi, J.-Y.; Lee, Y. H. Efficient Reduction of Graphite Oxide by Sodium Borohydride and Its Effect on Electrical Conductance. *Adv. Funct. Mater.* **2009**, *19*, 1987−1992.
(14) Becerril, H. A.; Mao, J.; Liu, Z.; Stoltenberg, R. M.; Bao, Z.; Chen, Y. Evaluation of Solution-Processed Reduced Graphene Oxide Films as Transparent Conductors. *ACS Nano* **2008**, *2*, 463−470.
(15) Hernandez, Y.; Nicolosi, V.; Lotya, M.; Blighe, F. M.; Sun, Z.; De, S.; McGovern, I. T.; Holland, B.; Byrne, M.; Gun'Ko, Y. K.; Boland, J. J.; Niraj, P.; Duesberg, G.; Krishnamurthy, S.; Goodhue, R.; Hutchison, J.; Scardaci, V.; Ferrari, A. C.; Coleman, J. N. High-Yield Production of Graphene by Liquid-Phase Exfoliation of Graphite. *Nat. Nanotechnol.* **2008**, *3*, 563−568.
(16) Blake, P.; Brimicombe, P. D.; Nair, R. R.; Booth, T. J.; Jiang, D.; Schedin, F.; Ponomarenko, L. A.; Morozov, S. V.; Gleeson, H. F.; Hill, E. W.; Geim, A. K.; Novoselov, K. S. Graphene-Based Liquid Crystal Device. *Nano Lett.* **2008**, *8*, 1704−1708.
(17) Hamilton, C. E.; Lomeda, J. R.; Sun, Z.; Tour, J. M.; Barron, A. R. High-Yield Organic Dispersions of Unfunctionalized Graphene. *Nano Lett.* **2009**, *9*, 3460−3462.
(18) Bourlinos, A. B.; Georgakilas, V.; Zboril, R.; Steriotis, T. A.; Stubos, A. K. Liquid-Phase Exfoliation of Graphite Towards Solubilized Graphenes. *Small* **2009**, *5*, 1841−1845.
(19) Khan, U.; O'Neill, A.; Lotya, M.; De, S.; Coleman, J. N. High-Concentration Solvent Exfoliation of Graphene. *Small* **2010**, *6*, 864−871.
(20) Economopoulos, S. P.; Rotas, G.; Miyata, Y.; Shinohara, H.; Tagmatarchis, N. Exfoliation and Chemical Modification Using Microwave Irradiation Affording Highly Functionalized Graphene. *ACS Nano* **2010**, *4*, 7499−7507.
(21) Hernandez, Y.; Lotya, M.; Rickard, D.; Bergin, S. D.; Coleman, J. N. Measurement of Multicomponent Solubility Parameters for Graphene Facilitates Solvent Discovery. *Langmuir* **2009**, *26*, 3208−3213.
(22) Lotya, M.; Hernandez, Y.; King, P. J.; Smith, R. J.; Nicolosi, V.; Karlsson, L. S.; Blighe, F. M.; De, S.; Wang, Z.; McGovern, I. T.; Duesberg, G. S.; Coleman, J. N. Liquid Phase Production of Graphene by Exfoliation of Graphite in Surfactant/Water Solutions. *J. Am. Chem. Soc.* **2009**, *131*, 3611−3620.
(23) Green, A. A.; Hersam, M. C. Solution Phase Production of Graphene with Controlled Thickness via Density Differentiation. *Nano Lett.* **2009**, *9*, 4031−4036.
(24) Ronan, J. S.; Mustafa, L.; Jonathan, N. C. Importance of Repulsive Potential Barriers for the Dispersion of Graphene Using Surfactants. *New J. Phys.* **2010**, *12*, 125008.
(25) Guardia, L.; Fernández-Merino, M. J.; Paredes, J. I.; Solís-Fernández, P.; Villar-Rodil, S.; Martínez-Alonso, A.; Tascón, J. M. D. High-Throughput Production of Pristine Graphene in an Aqueous Dispersion Assisted by Non-Ionic Surfactants. *Carbon* **2011**, *49*, 1653−1662.
(26) Kim, D. S.; Lee, T.; Geckeler, K. E. Hole-Doped Single-Walled Carbon Nanotubes: Ornamenting with Gold Nanoparticles in Water. *Angew. Chem., Int. Ed.* **2006**, *45*, 104−107.
(27) Geckeler, K. E.; Nishide, H. *Advanced Nanomaterials*. Wiley−VCH: Weinheim, Germany: 2010.
(28) Geckeler, K. E.; Rosenberg, E. *Functional Nanomaterials*; American Scientific Publication, Valencia, USA, 2006.
(29) Nepal, D.; Sohn, J.-I.; Aicher, W. K.; Lee, S.; Geckeler, K. E. Supramolecular Conjugates of Carbon Nanotubes and DNA by a Solid-State Reaction. *Biomacromolecules* **2005**, *6*, 2919−2922.
(30) Nepal, D.; Geckeler, K. E. pH-Sensitive Dispersion and Debundling of Single-Walled Carbon Nanotubes: Lysozyme as a Tool. *Small* **2006**, *2*, 406−412.
(31) Sanchez, V. C.; Jachak, A.; Hurt, R. H.; Kane, A. B. Biological Interactions of Graphene-Family Nanomaterials: An Interdisciplinary Review. *Chem. Res. Toxicol.* **2011**, *25*, 15−34.
(32) Premkumar, T.; Geckeler, K. E. Graphene−DNA Hybrid Materials: Assembly, Applications, And Prospects. *Prog. Polym. Sci.* **2012**, *37*, 515−529.
(33) Antony, J.; Grimme, S. Structures and Interaction Energies of Stacked Graphene-Nucleobase Complexes. *Phys. Chem. Chem. Phys.* **2008**, *10*, 2722−2729.
(34) Panigrahi, S.; Bhattacharya, A.; Banerjee, S.; Bhattacharyya, D. Interaction of Nucleobases with Wrinkled Graphene Surface: Dispersion Corrected DFT and AFM Studies. *J. Phys. Chem. C* **2012**, *116*, 4374−4379.
(35) Liu, F.; Choi, J. Y.; Seo, T. S. DNA Mediated Water-Dispersible Graphene Fabrication and Gold Nanoparticle-Graphene Hybrid. *Chem. Commun.* **2010**, *46*, 2844−2846.
(36) Lv, W.; Guo, M.; Liang, M.-H.; Jin, F.-M.; Cui, L.; Zhi, L.; Yang, Q.-H. Graphene-DNA hybrids: Self-Assembly and Electrochemical Detection Performance. *J. Mater. Chem.* **2010**, *20*, 6668−6673.
(37) Patil, A. J.; Vickery, J. L.; Scott, T. B.; Mann, S. Aqueous Stabilization and Self-Assembly of Graphene Sheets into Layered Bio-Nanocomposites Using DNA. *Adv. Mater.* **2009**, *21*, 3159−3164.
(38) Sun, X.; Liu, Z.; Welsher, K.; Robinson, J.; Goodwin, A.; Zaric, S.; Dai, H. Nano-graphene Oxide for Cellular Imaging and Drug Delivery. *Nano Res.* **2008**, *1*, 203−212.
(39) Xu, H.; Zeiger, B. W.; Suslick, K. S. Sonochemical Synthesis of Nanomaterials. *Chem. Soc. Rev.* **2013**, *42*, 2555−2567.
(40) Burnett, T. L.; Yakimova, R.; Kazakova, O. Identification of Epitaxial Graphene Domains and Adsorbed Species in Ambient Conditions Using Quantified Topography Measurements. *J. Appl. Phys.* **2012**, *112*, 054308−7.
(41) Sun, Z.; Hasan, T.; Torrisi, F.; Popa, D.; Privitera, G.; Wang, F.; Bonaccorso, F.; Basko, D. M.; Ferrari, A. C. Graphene Mode-Locked Ultrafast Laser. *ACS Nano* **2010**, *4*, 803−810.
(42) Cancado, L. G.; Takai, K.; Enoki, T.; Endo, M.; Kim, Y. A.; Mizusaki, H.; Jorio, A.; Coelho, L. N.; Magalhaes-Paniago, R.; Pimenta, M. A. General Equation for the Determination of the Crystallite Size L_a of Nanographite by Raman Spectroscopy. *Appl. Phys. Lett.* **2006**, *88*, 163106.
(43) Cho, E. C.; Xie, J.; Wurm, P. A.; Xia, Y. Understanding the Role of Surface Charges in Cellular Adsorption versus Internalization by Selectively Removing Gold Nanoparticles on the Cell Surface with a I2/KI Etchant. *Nano Lett.* **2009**, *9*, 1080−1084.

(44) Mutsaers, SE; P., J. Surface Charge of Macrophages and Their Interaction with Charged Particles. *J Leukoc Biol* **1998**, *44*, 17−20.
(45) Wilhelm, C.; Billotey, C.; Roger, J.; Pons, J. N.; Bacri, J. C.; Gazeau, F. Intracellular Uptake of Anionic Superparamagnetic Nanoparticles As a Function of Their Surface Coating. *Biomaterials* **2003**, *24*, 1001−1011.
(46) Ganta, S.; Devalapally, H.; Shahiwala, A.; Amiji, M. A Review of Stimuli-Responsive Nanocarriers for Drug and Gene Delivery. *J. Controlled Release* **2008**, *126*, 187−204.
(47) Yamaguchi, H.; Wyckoff, J.; Condeelis, J. Cell Migration in Tumors. *Curr. Opin. Cell Biol.* **2005**, *17*, 559−564.
(48) Konantz, M.; Balci, T. B.; Hartwig, U. F.; Dellaire, G.; André, M. C.; Berman, J. N.; Lengerke, C. Zebrafish Xenografts As a Tool for in Vivo Studies on Human Cancer. *Ann. N.Y. Acad. Sci.* **2012**, *1266*, 124−137.
(49) Jung, D.-W.; Oh, E.-S.; Park, S.-H.; Chang, Y.-T.; Kim, C.-H.; Choi, S.-Y.; Williams, D. R. A Novel Zebrafish Human Tumor Xenograft Model Validated for Anti-Cancer Drug Screening. *Mol. Biosyst.* **2012**, *8*, 1930−1939.
(50) Sipes, N. S.; Padilla, S.; Knudsen, T. B. Zebrafish - As an integrative Model for Twenty-First Century Toxicity Testing. *Birth Defects Res., Part C* **2011**, *93*, 256−267.
(51) Cui, S.; Mao, S.; Lu, G.; Chen, J. Graphene Coupled with Nanocrystals: Opportunities and Challenges for Energy and Sensing Applications. *J. Phys. Chem. Lett.* **2013**, *4*, 2441−2454.
(52) Xi, Q.; Chen, X.; Evans, D. G.; Yang, W. Gold Nanoparticle-Embedded Porous Graphene Thin Films Fabricated via Layer-by-Layer Self-Assembly and Subsequent Thermal Annealing for Electrochemical Sensing. *Langmuir* **2012**, *28*, 9885−9892.